Influence of particle size and concentration on the diffuse backscattering of polarized light from tissue phantoms and biological cell suspensions

Andreas H. Hielscher, Judith R. Mourant, and Irving J. Bigio

We present experimental results that show the spatial variations of the diffuse-backscattered intensity when linearly polarized light is incident upon highly scattering media. Experiments on polystyrene-sphere and Intralipid suspensions demonstrate that the radial and azimuthal variations of the observed pattern depend on the concentration, size, and anisotropy factor *g* of the particles that constitute the scattering medium. Measurements performed on biological-cell suspensions show the potential of this method for cell characterization. © 1997 Optical Society of America

Key words: Polarization, multiple scattering, optical diagnostics for medicine.

1. Introduction

That polarization effects in scattered light can yield useful information about biological material was shown as early as 1976, when Bickel *et al.* announced a "new biophysical tool."[1] They investigated how suspensions of *Bacillus Subtilis* affect the angular distribution of polarized light by measuring various components of the scattering matrix[2] for scattering angles between 3° and 165°. Similar studies on other bacterial suspensions were later performed by van de Merwe *et al.*[3] and Bronk *et al.*[4,5] The use of polarized light scattering for biological-cell differentiation was again first demonstrated by Bickel *et al.*[6] deGrooth *et al.*[7] showed that depolarization of linearly polarized light can be used in flow cytometers to distinguish among a number of leukocyte types.[8] Furthermore, polarized light has been employed to study polynucleosome superstructures[9] and other biomolecular structures.[10]

All the above-mentioned applications of polarized light require measurement of polarized irradiance over a broad range of forward-scattering angles. However, there are many biomedical applications in which the properties of backward-scattered light are of interest. For example, only backscattered light is available in endoscopic procedures that are used to diagnose tissues. A few studies exist that approach this problem. Recently Mishchenko and Hovenier[11] described theoretically the depolarization of light backscattered from a randomly oriented nonspherical particle. In another theoretical study, McCormick[12] suggested a method to retrieve the particle-size distribution in an optically thick plane-parallel aerosol. His proposed procedure requires a time-dependent measurement of the backscattered polarized irradiance and could potentially also be applied to biological samples. Time-resolved measurements of the depolarization of multiple backscattered light from turbid media were performed by Yoo and Alfano.[13] In their experiments, 5-fs laser pulses, which were linearly polarized and collimated to a diameter of 5 mm, were directed onto latex-bead suspensions. The backscattered light within the beam area was collected and recorded as a function of time. Yoo and Alfano observed that the depolarization varies with particle size and concentration, and they estimated that approximately 20 scattering events are necessary to depolarize the light completely. Anderson[14] used linearly polarized light to illuminate the skin of his patients broadly. Viewing the skin through another linear polarizer, he could distinguish the reflectance from the skin surface, which preserves the plane of polarization, and the light backscattered from within the tissue, which is more likely to change the plane of polarization or become depolarized.

In this paper we investigate the behavior of diffuse-

The authors are with Los Alamos National Laboratory, Bioscience and Biotechnology, CST-4, MS E535, Los Alamos, New Mexico 87545.

Received 17 April 1996; revised manuscript received 27 August 1996.
0003-6935/97/010125-11$10.00/0

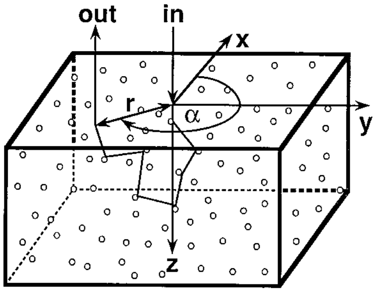

Fig. 1. Illustration of the sample geometry for measurement of diffuse-backscattered polarized light.

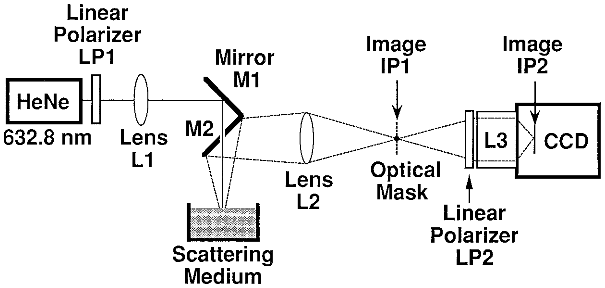

Fig. 2. Experimental setup for measuring diffuse-backscattered polarized light.

backscattered, linearly polarized, continuous light from turbid tissue phantoms and biological suspensions. The difference between diffuse-backscattered polarized light and backscattered polarized light as described in the paragraph above is best illustrated in Fig. 1. Instead of using a broad beam for sample illumination, we focused the linearly polarized laser beam to a small spot with a diameter of typically <500 μm on the surface of the sample. This geometry is more likely in endoscopic procedures in which light is guided through an optical fiber to the area of interest. We define as diffuse-backscattered light the light that has been scattered multiple times inside the medium and escapes the medium at a surface point that is given by a lateral distance r from the laser input point and an angle α measured from the x axis (Fig. 1). Recently, Wang *et al.*[15] and Jacques *et al.*[16] reported on azimuthal variations of intensity in the diffuse-backscattered linearly polarized light around the light input point when viewed through a polarizing filter. They found that these azimuthal variations vanished at approximately two transport mean free paths (mfp's) $\{\mathrm{mfp}' = 1/[\mu_s(1 - g)]\}$ from the initial laser spot. For larger distances r, an exponential decay in the light intensity is observed that is comparable with the case in which no polarizers are used.[17] Dogariu and Asakura[18] used the azimuthal intensity variations in the polarized backscattered light for the determination of the average photon path length in a scattering medium. In the work presented here, we experimentally study in detail the effects of particle size, concentration, and scattering-anisotropy factor g on the diffuse backscattering of linearly polarized light. We demonstrate that differences in particle size, concentration, and g value lead to differences in the spatial pattern of backscattered light when viewed through a polarizer.

First we describe the experimental setup and discuss the data processing and analysis. We then show results from polystyrene-sphere suspensions that contain just one size of particle, which have all the same refractive index. The particle sizes and concentrations are varied, and the variations in the observed intensity patterns of the diffuse-backscattered light are reported. This is followed by measurements on Intralipid suspensions that contain particles of varying sizes. Finally, we report on measurements made on yeast and fibroblast suspensions. These measurements demonstrate that diffuse-backscattered linearly polarized light yields information about the scattering centers in these types of suspension and can be useful in characterizing biological cells.

2. Methods

A. Experimental Setup

The experimental setup for studying the diffuse backreflectance of polarized light is depicted in Fig. 2. A He–Ne laser with an output power of 5 mW at a wavelength of $\lambda = 632.8$ nm was used as a light source. Linear polarizer LP1 was placed in front of the He–Ne laser. The polarized light was focused by lens L1 ($f = 15$ cm) and mirror M1 onto the surface of the turbid medium through a hole in the center of mirror M2. Lens L2 ($f = 15$ cm) was used to generate an image of the surface area around the input point in image plane IP1. This intermediate image plane allows us to place an optical mask in the center of this image and in this way reject the strong specular reflection from the surface at the laser input point. The mask had, typically, a diameter of 1 mm; however, it could be varied up to 5 mm. The image at IP1 including the optical mask was viewed with a 55-mm Nikon camera lens L3 (Micro-Nikkor, 55 mm, $f/2.8$), which was mounted on a cooled, intensified CCD camera (Princeton Instrument, Inc., 3660 Quakerbridge Rd., Trenton, N.J. 08619). The CCD chip had 575×384 pixels with a pixel size of 20×20 μm. The surface area under observation around the laser entrance point could be varied from 0.5 cm × 0.5 cm to 4 cm × 4 cm, depending on the position of L2 and L3. Polarizer LP2 was placed in front of L3 to serve as an analyzer. The CCD camera was controlled and operated with IPLab software (Signal Analytics Cooperation, 374 Maple Ave. East, Suite #204, Vienna, Va. 22180-4718) running on a Mac-IIci. The dynamic range of the CCD camera was 12 bits. Below we refer to images obtained with this setup as polarized-diffuse-backscattering (PDB) images.

B. Phantom and Cell Preparation

1. *Polystyrene-Sphere and Intralipid Suspensions*

We used aqueous polystyrene-sphere suspensions as tissue phantoms that contain only one type of scattering center. For this study we used spheres with eight different diameters (0.096, 0.204, 0.304, 0.497, 0.966, 2.04, 2.92, and 10.2 μm), which were suspended in deionized H_2O with trace amounts of surfactants (Duke Scientific Corporation, 2463 Faber Place, P.O. Box 50005, Palo Alto, Calif. 94303). We varied the concentrations of solids by weight from 0.003% to 3.0%. The index of refraction of the spheres was 1.59 at 632.8 nm and the density was 1.05 g/ml.

We also used Intralipid (Kabi Pharmacia Inc., Clayton, N.C. 27520, Lot NR17230) in various concentrations as a tissue phantom with scattering centers of a known size distribution. Intralipid is a fat emulsion consisting of phospholipid micelles and water, which is used clinically as an intravenously administered nutrient. Because Intralipid has no strong absorption bands in the visible region of the electromagnetic spectrum and because it is readily available and inexpensive, it is often used as a tissue-simulating phantom medium. Its optical properties have been studied in detail by several authors.[19–22] Van Staveren *et al.*[21] determined the particle-size distribution and calculated the mean particle diameter to be 97 nm. They found particles as large as 675 nm and smaller than 25 nm in their Intralipid suspension. From their data the standard deviation (SD) can be estimated to be approximately 101 nm (104%). For the SD, in this paper we follow the definition given by Press *et al.*[23]

2. *Yeast-Cell Suspensions*

Yeast-cell suspensions were investigated as an example for biological cells. Wild-type yeast cells (*Saccharomyces cerevisiae*) were aerobically grown in a liquid medium containing 1% yeast extract (Difco Lab., Detroit, Mich.), 0.12% $(NH_4)_2SO_4$, and 0.1% KPO_4 (pH 7.0) supplemented with either 2% ethanol or 5.6% glucose as a C source.

Cells were harvested at the midexponential growth phase, centrifuged, and washed twice in cold H_2O. The cells were then suspended at different concentrations [(20–50 mg dry wt)/ml] in a solution containing 2-mM KPO_4, 2-mM $MgSO_4$, 1.7-mM NaCl, and 50-mM *mes*-NaOH, pH 6.1. The optical properties of these cell suspensions for concentrations of 15–46 (mg dry weight)/ml were recently reported to lie in the range of $\mu_s' = 3$–8.5 cm^{-1} and $\mu_a = 0.045$–0.065 cm^{-1}.[24] For several different suspensions, the mean cell diameter was between 4.7 and 5.5 μm, with standard deviations ranging from 3.5% to 6.3%.

3. *Rat Fibroblast Suspensions*

As an example for mammalian cells, measurements were also performed on rat fibroblast M1 cell suspensions. The fibroblast is the cell most commonly found in connective tissue. It is responsible for the synthesis of fibers and amorphous intercellular substances. Fibroblasts are rich in mitochondria, lipid droplets, Golgi complexes, and rough endoplasmic reticulum.[25]

Rat fibroblast M1 cells were cultured in an α-minimal essential medium containing 10% bovine calf serum, penicillin, and streptomycin in a humidified incubator at 37 °C equilibrated with 5% CO_2 in 95% air (pH 7.4). Monolayer cultures were propagated in tissue culture flasks, as described in detail elsewhere,[26] to maintain cell growth and viability. Cell suspensions for optical measurements were prepared by the dissociation of cells from the culture surface by treatment with 0.25% Trypsin in a Ca- and Mg-free buffer at pH 7.4 for 10 min at 37 °C. An excess ice-cold complete medium was then added, the mixture was mixed by repeated passage through a pipet, a sample was removed for counting, and the cell suspension was centrifuged at 1500 rpm for 10 min. The cell pellet was then resuspended in an ice-cold phosphate-buffered saline at a concentration of approximately 5.0×10^7 cells/ml and stored on ice until the optical measurements. Cells were counted with an electronic particle counter equipped with a system for recording the volume distribution of the particles. Only those particles within the cell volume distribution were counted, and the mean volume of the cell population was estimated as the mean of the volume distribution of $>10^4$ cells.[26] The mean cell diameter for various samples was between 13 and 16 μm, with standard deviations ranging from 6.5% to 11%. Fibroblast and yeast cells in suspension tend to assume a spherical shape, which was confirmed with microscopic observation.

C. Data Processing and Analysis

1. *Data Processing*

To quantify the surface images taken from the various scattering media, a spatial calibration was performed by the placement of a millimeter-resolution standard (Edmund Scientific, Barrington, N.J. 08007-1380; U.S. Air Force Optical Test Pattern 38710) on the surface of the sample. Under white-light illumination an image was acquired with the CCD camera and stored as reference. Furthermore, dark measurements with a closed shutter in front of the CCD camera were taken to determine the background signal, which was to be subtracted from all images before further data processing. We determined the response function of the CCD camera by shining light into the camera and successively placing neutral-density filters in front of the camera until the signal level reached the dark level. This procedure was repeated for several values of the internal camera amplification, and the images were corrected accordingly.

Three types of image of the surface of the scattering medium around the light input point were taken: (1) linear polarizers LP1 and LP2 removed (I_t), (2) LP1 and LP2 crossed with respect to each other (I_x), and (3) LP1 and LP2 parallel with respect to each other (I_p). The images taken with polarizers were divided point by point by the images taken without polarizers to yield the intensity ratios:

$$I_{p,t}(r, \alpha) = \frac{I_p(r, \alpha)}{I_t(r, \alpha)}, \tag{1a}$$

$$I_{x,t}(r, \alpha) = \frac{I_x(r, \alpha)}{I_t(r, \alpha)}. \tag{1b}$$

By normalizing against I_t, we eliminate effects that are caused by the r-dependent exponential intensity decay. This decay is typical in multiple-scattering media for point illumination by a continuous light source.[17] Therefore the chosen normalization ensures that only effects that are due to the linear polarization of the light are observed.

In order to eliminate so-called salt-and-pepper noise, a 3 × 3 median filter[27] was applied to the calculated images of the intensity ratios. Salt-and-pepper noise arises from noisy sensor or electrical transmission errors and usually appears as discrete, isolated, strong pixel variations that are not spatially correlated. The median filter used in this work assigns the median value of the nine pixels of a 3 × 3 square to the center pixel and effectively eliminates discrete, isolated strong pixel variations. A spatial low-pass filter, which assigns the mean value of the nine pixels of a 3 × 3 square to the center pixel, was used to smooth the data further. Finally, the contrast of the displayed images was enhanced by the application of a histogram equalization[28] and a multibanded gray scale.

2. *Example*

To illustrate the image processing, two examples of our measurements are shown in Figs. 3(a) and 3(b). The PDB images display intensities of diffuse-backscattered light for a surface area of 1.75 cm × 1.75 cm, which images to 320 × 320 pixels on the CCD. The light is linearly polarized along the x axis and enters the medium in the center of all figures. As can be seen, this center is obscured by a circular mask, which rejects the specular reflection of the laser spot from the surface of the medium. The linelike disturbance that enters the pictures from the left is caused by a 0.5-mm-diameter needle used to hold the mask. Figure 3(a) is the result of a measurement on a yeast-cell suspension with polarizers LP1 and LP2 crossed. Figure 3(b) shows the same suspension, however, with LP1 and LP2 removed.

With no polarizers present [Fig. 3(b)] the intensity is highest in the center around the mask and decays exponentially with distance from the center.[17] There is no azimuthal dependence of the intensity. With crossed polarizers [Fig. 3(a)] a strong azimuthal dependence appears with maxima at ± 45° and ± 135°. This azimuthal dependence disappears at some distance from the center, after which the simple exponential radial dependence dominates. The result of a point-by-point division of Fig. 3(a) by Fig. 3(b), the intensity ratio $I_{x,t}(r, \alpha)$ is shown in Fig. 3(c). Instead of four maxima at ± 45° and ± 135°, minima with values smaller than 1 appear at 0° and 90°. Toward the edges of the image the ratio becomes 1. It can be seen that, in Fig. 3(a), the azimuthal dependence seems to disappear at $r = 0.5$ cm from the center, whereas in Fig. 3(c) the azimuthal dependence is clearly still visible at $r = 0.8$ cm.

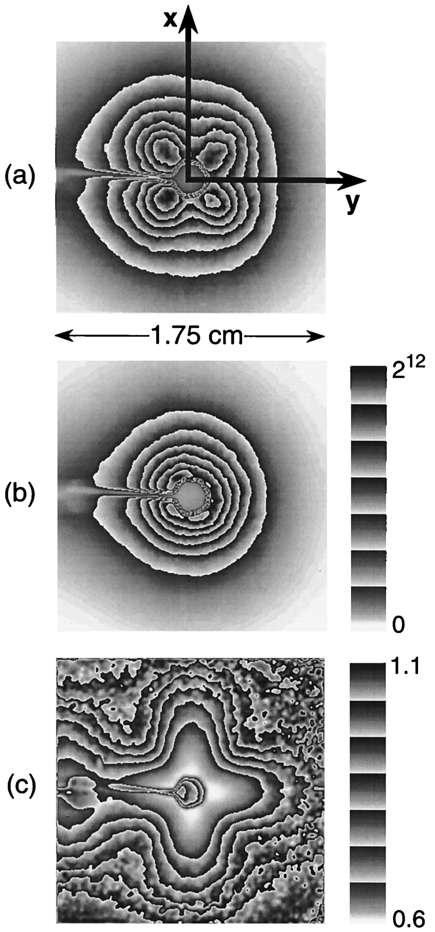

Fig. 3. (a) Image of the diffuse-backscattered intensity from a yeast cell suspension taken with crossed polarizers LP1 and LP2, (b) image of the diffuse-backscattered intensity from a yeast-cell suspension taken without polarizers, (c) point-by-point division of the image in (a) by image in (b). This image was additionally rendered by filter operations and contrast enhancement.

3. *Data Analysis*

The question arises: How can these images be used to gain information about the scattering medium? Below we investigate how the azimuthal and radial dependences of patterns like those in Fig. 3(c) are influenced by the size, the anisotropy factor g, and the concentration of the particles responsible for the scattering.

To quantify these influences we turn to polystyrene-sphere suspensions with spheres of known diameter d and concentration or number density N_s. We have used Mie theory[29] to calculate the scattering phase function $p(\Omega, \Omega')$, which describes the probability that during a scattering event a photon with initial direction Ω' is scattered in the direc-

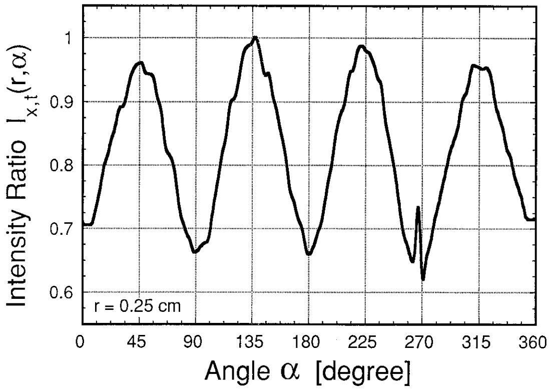

Fig. 4. Values of the intensity ratio [Fig. 3(a)/Fig. 3(b)] on a circle with radius $r = 0.25$ cm, centered around the light input point in the middle of Fig. 3(c).

tion Ω. Subsequently the anisotropy factor g was determined, which is defined as

$$g \equiv \int_{4\pi} \Omega \cdot \Omega' \, p(\Omega, \Omega') \, d\Omega'. \tag{2}$$

Furthermore, Mie theory was used to calculate the scattering cross section C_s of the individual particles. Given the number density N_s, the scattering coefficient can be determined as $\mu_s = N_s C_s$. The inverse of μ_s gives the average distance between two scattering events, also called the mfp. Finally, we also calculate the reduced scattering coefficient $\mu_s' = (1 - g)\mu_s$. The transport mfp (mfp′) is defined as the inverse of μ_s'.

We determined the pattern size by looking at the azimuthal variations (angle α in Fig. 1) of the backscattered intensity ratio $I_{x,t}$ or $I_{p,t}$ at a radius r from the light input spot. In Fig. 4 this ratio is shown for a circle with radius $r = 0.25$ cm centered in the middle of Fig. 3(c). The spike at 270° is caused by the holder of the optical mask and may be ignored. For this example the azimuthal variations are stronger than 30%. We define the radius at which these azimuthal variations become smaller than 5% as the pattern size r_p. This definition was chosen because the noise level in our images is approximately 5%. Other definitions (e.g., 2%, 10%) are possible and will not change the basic results of this study, as discussed below.

3. Results

A. Polystyrene-Sphere Suspensions

1. *Influence of Sphere Size*

We first investigated how the diffuse-backscattered light is influenced by the particle size. Figure 5 shows intensity ratio images from three suspensions that contain polystyrene spheres with different diameters. Instead of the whole images as in Fig. 3, only the right halves of the figures are shown because all the images are symmetric with respect to the x axes.

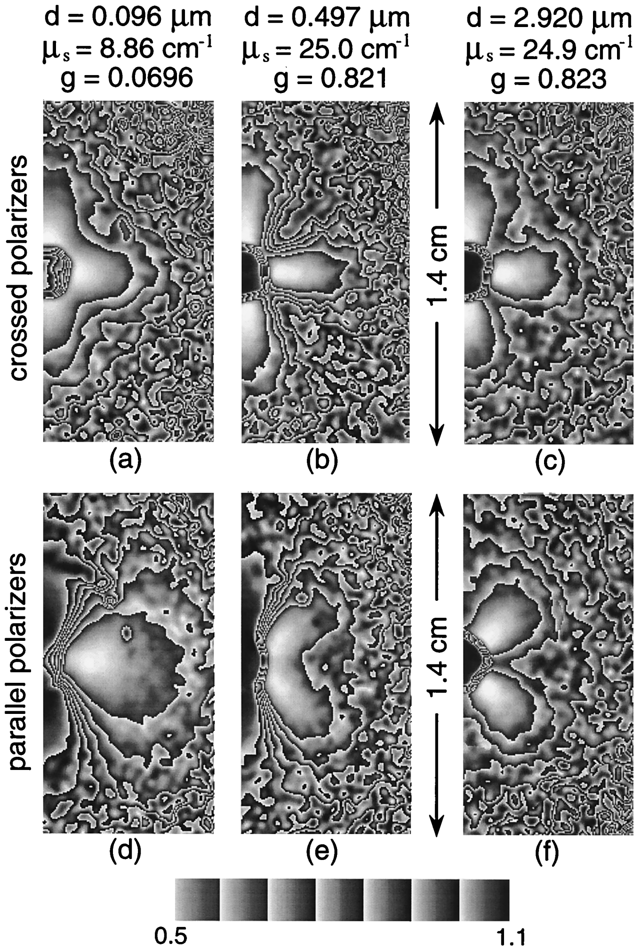

Fig. 5. Two-dimensional intensity ratios $I_{x,t}(r, \alpha)$ and $I_{p,t}(r, \alpha)$ calculated from PDB images of polystyrene-sphere solutions with (a), (b), (c) crossed polarizers, (d), (e), (f) parallel polarizers. The column pairs [(a), (d)], [(b), (e)], and [(c), (f)] have the same sphere diameter d, scattering coefficient μ_s, and anisotropy factor g, respectively.

The images $I_{x,t}(r, \alpha)$ in Figs. 5(a)–5(c) were obtained with crossed polarizers, whereas the images $I_{p,t}(r, \alpha)$ in Figs. 5(d)–5(f) were obtained with parallel polarizers. Compared with the wavelength of the He–Ne laser that was used in these experiments, the diameters d of the spheres are several times smaller [Figs. 5(a) and 5(d): $d = 0.096$ µm with SD = 0.0053 µm], similar [Figs. 5(b) and 5(e): $d = 0.497$ µm, SD = 0.0056 µm], and several times larger [Figs. 5(c) and 5(f): $d = 2.92$ µm, SD = 0.04 µm]. Moreover, it should be noted that the suspensions of Figs. 5(b), 5(e) and 5(c), 5(f) have almost the same scattering coefficient μ_s, 25.0 cm^{-1} and 24.9 cm^{-1}, respectively, and similar anisotropy factors g, 0.821 and 0.823, respectively, at the He–Ne wavelength $\lambda = 632.8$ nm.

The azimuthal structure in the case of crossed polarizers [Figs. 5(a)–5(c)] does not have a strong dependence on the particle size. Although the shapes of the minima lobes differ slightly, the angles at which they occur are, in all three cases, the same at 0° and 90°. In the case of parallel polarizers [Figs.

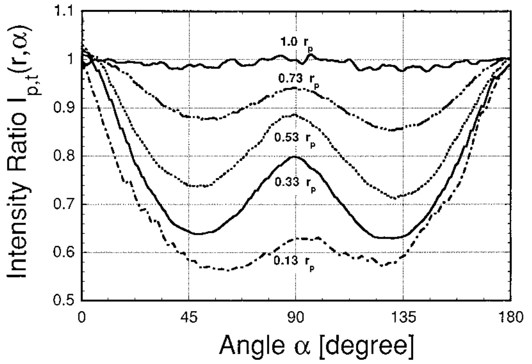

Fig. 6. Intensity ratios $I_{p,t}(r, \alpha)$ as functions of azimuthal angle α for various radii $r \le r_p$. Here the results of a polystyrene-sphere suspension with sphere diameter $d = 0.966$ μm are shown.

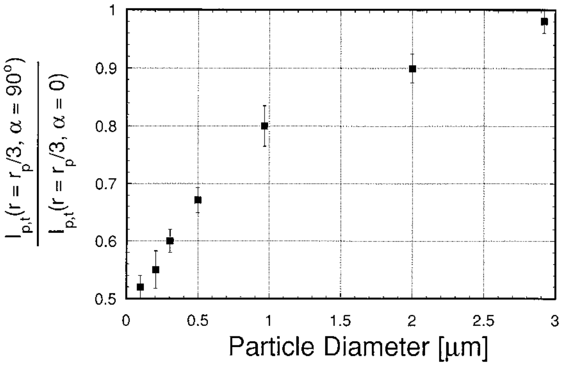

Fig. 8. Dependence of the ratio of $I_{p,t}(r = r_p/3, \alpha = 90°)/I_{p,t}(r = r_p/3, \alpha = 0°)$ on the particle diameter in polystyrene-sphere suspensions.

5(d)–5(f)] more pronounced differences in the azimuthal distributions can be observed. For the largest spheres [Fig. 5(f)], two minima can be found at 45° and 135° with respect to the polarization of the incoming light (Fig. 3). The cross pattern appears to have been rotated by 45° when compared with the pattern in Fig. 5(c). The sphere suspension with almost the same μ_s and g but different particle size [Fig. 5(e)] displays a different pattern. Minima still occur at 45° and 135°; however, the minima are much broader and for small r extend also in the 90° direction to form a butterflylike pattern. For the suspension with even smaller particles [Fig. 5(d)] this extension at 90° has become so strong that only one minimum is visible, and the cross structure disappears.

Rather than a two-dimensional (2D) image of the sample surface around the light input point, Fig. 6 shows the intensity ratios for various fractions of the radius of the pattern size r_p as a function of the azimuthal angle α. Here the results of a polystyrene-sphere suspension with sphere diameter $d = 0.966$ μm (SD = 0.6%) are shown. It can be seen that the difference in the intensity between 0° and 90° increases as the fraction decreases. This was observed for all particle sizes.

Figure 7 displays the intensity ratios of Figs. 5(d)–5(f) and 6 for the fixed radius of $r = r_p/3$ as functions of the azimuthal angle α. The radius $r_p/3$ was chosen because we found that for smaller radii the distortions caused by the optical mask increase, whereas for larger radii, as shown in Fig. 6, the variations in the intensity ratios as functions of angle decrease. Figure 7 shows that for an increasing particle size the minimum at 90° becomes a local maxima and two new minima at 45° and 135° appear. This holds true not only for $r = r_p/3$ but for all radii $r < r_p$.

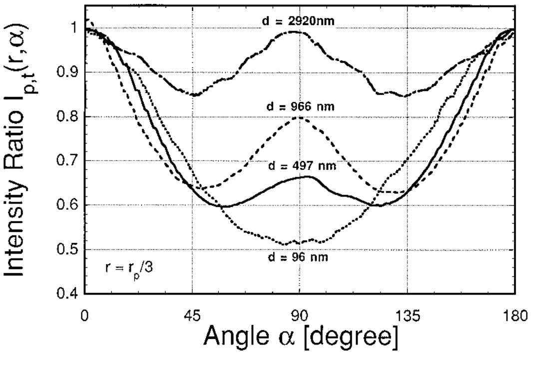

Fig. 7. Intensity ratios $I_{p,t}(r, \alpha)$ of Figs. 5(d)–5(f) and 6 for a fixed radius of $r = r_p/3$ as functions of the azimuthal angle α.

In general it can be concluded that the ratio of the intensities at 0° and 90°, for any given radius $r < r_p$, is related to the size of scattering particles in the suspension. In Fig. 8 the ratios of the intensities at 0° and 90° for seven polystyrene-sphere suspensions with different particle diameters are displayed. For particle sizes larger than 3 μm this ratio was 1. As radius we chose here again $r = r_p/3$. If a larger radius is chosen, the curve is shifted up toward 1, whereas for smaller radii the curve shifts to lower values. Similarly, the curve will shift if the definition of the pattern size r_p is changed.

2. *Influence of Concentration and* g*-Value*

In all our experiments we observed that changing the concentration of the sphere suspensions, or in other words, changing the macroscopic scattering coefficient μ_s, does not change the azimuthal dependence. However, the particle concentrations affect the pattern size r_p. Increasing the concentration of particles in the solution by a factor of n led to a decrease of the pattern radius r_p by a factor of n. An example is shown in Fig. 9. Here the pattern radius for the case of crossed polarizers was determined for polystyrene-sphere suspensions with a particle diameter of $d = 0.497$ μm. The concentration was varied from 0.075% to 0.186% solid weight of polystyrene spheres. The corresponding scattering coefficients μ_s were calculated from Mie theory and are provided in the scale on the top of the graph. It can be seen, for example, that doubling the concentration from 0.093% to 0.186% approximately halves the radius r_p from 0.61 to 0.31 cm.

Furthermore we found that r_p also depends on the

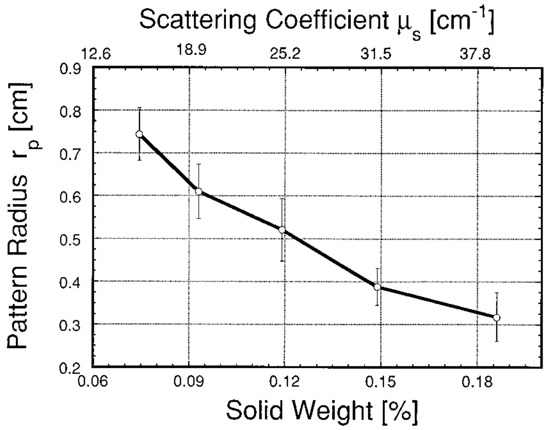

Fig. 9. Pattern radius $r_{x,p}$ for the case of crossed polarizers for polystyrene-sphere suspensions with a particle diameter of $d = 0.497$ μm as a function of particle concentration.

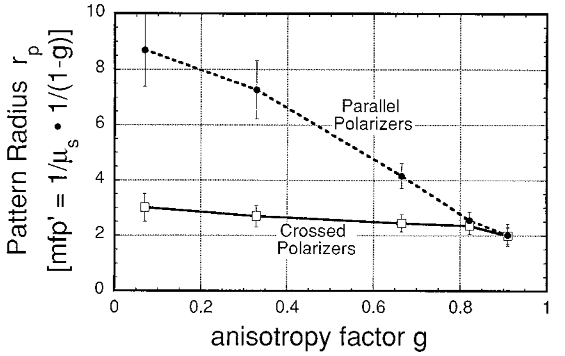

Fig. 11. Radius of the polarization pattern and its dependence on the anisotropy factor g for the cases of crossed polarizers (open squares, solid curve) and parallel polarizers (filled circles, dashed curve).

anisotropy factor g of the particles in the suspensions. Results of measurements with crossed polarizers on three suspensions with similar scattering coefficients μ_s but different g values are displayed in Fig. 10. The anisotropy factor g increases from $g = 0.329$ [Fig. 10(a)] to $g = 0.663$ [Fig. 10(b)] to $g = 0.821$ [Fig. 10(c)]. A comparison of the three figures shows that with increasing g the radius of the pattern increases.

In Fig. 11 the radii of the patterns for crossed and parallel polarizers are displayed as functions of the g value. As units for r_p we chose the transport mfp, $\text{mfp}' = [(1 - g)\mu_s]^{-1}$. Given these units, r_p depends weakly on g for the case of crossed polarizers. A much stronger dependence on g can be observed for the case of parallel polarizers. For decreasing g values the parallel pattern increasingly exceeds the size of the crossed pattern, whereas for increasing g values the pattern sizes approach each other. If $g = 1$, the unit mfp′ becomes infinite, and therefore r_p should become 0 for both the parallel and the crossed polarizer cases. Furthermore it should be noted that using a different definition for the pattern radius r_p will shift these curves slightly; however, it does not change the overall dependence of r_p on g.

We conclude that, by measuring the radius of the polarization pattern for crossed and parallel polarizers, we can estimate μ_s and g of a turbid suspension for a given index of refraction and wavelength. The ratio of the radii of the images taken with parallel and crossed polarizers yields a value for g. From Fig. 11 and the measurement of the radius of the crossed or parallel pattern, we can then determine μ_s. Furthermore, as discussed in the section on azimuthal dependence (Subsection 3.A.1., Fig. 8), the image with the parallel polarizer yields information about the diameter d of the particle responsible for the scattering. In Subsection 3.B below, an example illustrates these methods for the estimation of d, g, and μ_s.

B. Intralipid Suspensions

To see if these patterns are still observable in suspensions with a range of particle sizes, we studied

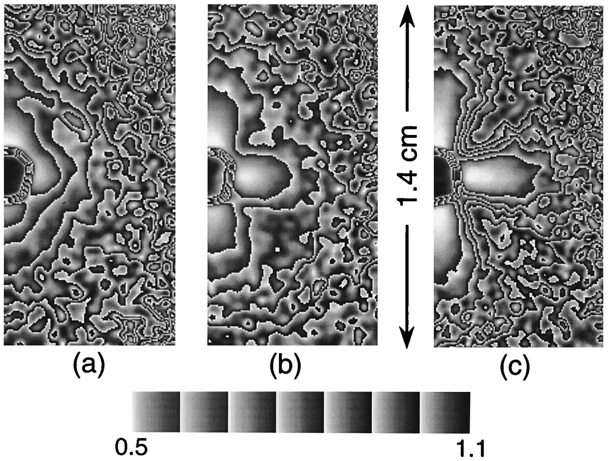

Fig. 10. 2D intensity ratios $I_{x,t}(r, \alpha)$ as calculated from images of a polystyrene-sphere suspension with crossed polarizers: (a) $g = 0.329$, $\mu_s = 27.9\ \text{cm}^{-1}$, $d = 0.204$ μm; (b) $g = 0.663$, $\mu_s = 26.2\ \text{cm}^{-1}$, $d = 0.304$ μm; (c) $g = 0.821$, $\mu_s = 24.9\ \text{cm}^{-1}$, $d = 0.497$ μm.

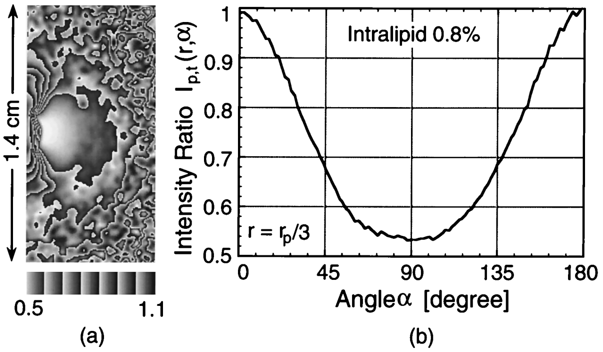

Fig. 12. Intensity ratio $I_{p,t}(r, \alpha)$ obtained from a 0.8% Intralipid solution with parallel polarizers: (a) 2D image, (b) one-dimensional graph with radius fixed at $r = r_p/3 = 0.15$ cm. In both cases $0 \leq \alpha \leq 180°$.

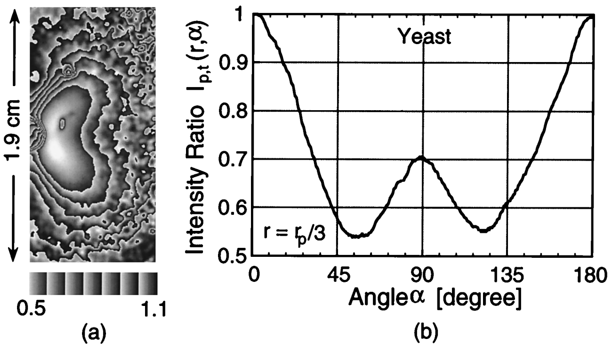

Fig. 13. Intensity ratio $I_{p,t}(r, \alpha)$ obtained from a wild-type yeast cell-suspension [(50 mg dry weight)/ml] with parallel polarizers: (a) 2D image, (b) one-dimensional graph with radius fixed at $r = r_p/3 = 0.38$. In both cases $0 \le \alpha \le 180°$.

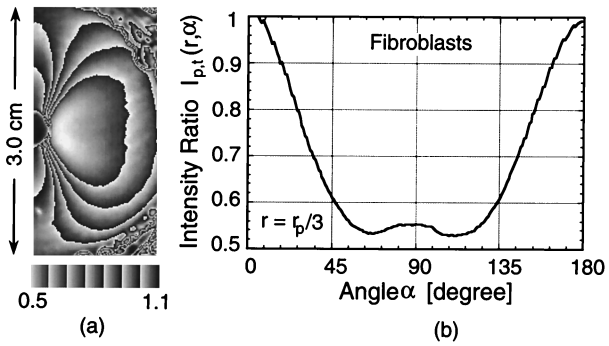

Fig. 14. Intensity ratio $I_{p,t}(r, \alpha)$ obtained from an M1 rat fibroblast-cell suspension with parallel polarizers: (a) 2D image, (b) one-dimensional graph with radius fixed at $r = r_p/3 = 0.68$ cm. In both cases $0 \le \alpha \le 180°$.

Intralipid solutions. In Fig. 12(a) the intensity ratio $I_{p,t}(r, \alpha)$ is shown for a 0.8% Intralipid suspension. Figure 12(b) shows the azimuthal variation of $I_{p,t}$ for $r = r_p/3 = 0.15$ cm. When Figs. 12(a) and 12(b) are compared with Figs. 5(d) and 7, it can be seen that the polarization intensity pattern from the Intralipid suspension is similar to that observed with the polystyrene-sphere suspension with a particle diameter of 96 nm. As mentioned above the mean particle diameter in the Intralipid suspension is 97 nm. The ratio between the intensities at 90° and 0° of the Intralipid suspension yields 0.53 [Fig. 12(b)]; using the polystyrene-sphere calibration curve (Fig. 8), we find that this corresponds to a particle diameter of 110 nm (±20 nm). It appears that the pattern structure observed with mixed-size suspensions is approximated by the pattern observed with a single-size suspension, in which the particles have a diameter similar to the mean diameter of the mixed-size suspensions.

Other optical parameters of the suspension can be estimated as follows: The ratio $R_{x,p}$ of the crossed pattern radius $r_{p,x}$ divided by the parallel pattern radius $r_{p,p}$ is $R_{x,p} = (r_{p,x})/(r_{p,p}) = 0.75$. From Fig. 11 we find that if $R_{x,p} = 0.75$, the anisotropy factor g is ~0.76. Furthermore, Fig. 11 shows that if $g = 0.76$, the radius of the parallel pattern is approximately $r_{p,p} = 3.2$ mfp′. From Fig. 12(a) we measure the radius of the parallel pattern as $r_{p,p} = 0.45$ cm and get

$$\begin{aligned} r_{p,p} &= 0.45 \text{ cm} = 3.2 \text{ mfp}' \\ &= 3.2\,[(1-g)\mu_s]^{-1} \Rightarrow \mu_s = 29.6 \text{ cm}^{-1}. \end{aligned}$$

These values for g and μ_s for a 0.8% Intralipid suspension, measured at a wavelength of $\lambda = 632.8$ nm, lie well within the range of values previously found in other studies (Flock *et al.*[22]: $g = 0.825$, $\mu_s = 27.2$; Moes *et al.*[20]: $g = 0.71$, $\mu_s = 30.88$; van Staveren *et al.*[21]: $g = 0.768$ (experimental), $g = 0.731$ (theoretical), $\mu_s = 38.08$; Star *et al.*[19]: $g = 0.83$, $\mu_s = 44.0$).

C. Biological-Cell Suspensions

1. *Yeast Cells*

As the first example of biological material we studied wild-type yeast-cell suspensions. In Subsection 2.C.2. we already showed the images for the crossed polarizer case. In Fig. 13(a) the related intensity ratio for parallel polarizers is shown, and Fig. 13(b) displays the azimuthal variations for $r = r_p/3 = 0.38$ cm. When Figs. 13(a) and 13(b) are compared with Figs. 5(e) and 7, it can be seen that the polarization intensity pattern from the yeast-cell suspension is similar to that observed with the polystyrene-sphere suspension with a particle diameter of 497 nm. The ratio between the intensities at 90° and 0° of the yeast-cell suspension yields 0.70; using the polystyrene-sphere calibration curve (Fig. 8), we find that this corresponds to a particle diameter of 600 nm (±70 nm). An analysis similar to that in Subsection 3.B reveals for this yeast suspension [(50 mg dry weight)/ml] an anisotropy factor of approximately $g = 0.8$ and a scattering coefficient of $\mu_s = 23.0$ cm^{-1}.

It is interesting to note that the yeast cells themselves had diameters in the range of approximately 3–8 μm [mean diameter 5.2 μm, SD = 0.3 μm (5.8%)]. Thus it appears that the cell volume cannot be responsible for most of the scattering. Smaller cell compartments like the nucleus, with a diameter of ~1 μm, or yeast-cell mitochondria, with a diameter of 0.2–0.5 μm,[30,31] appear to cause most of the light scattering.

2. *Rat Fibroblast Cells*

As an example for mammalian cells we investigated the diffuse backscattering of polarized light from M1 rat fibroblast-cell suspensions. In Fig. 14(a) the intensity ratio $I_{p,t}(r, \alpha)$ for parallel polarizers is shown. Figure 14(b) displays the azimuthal variations for $r = r_p/3 = 0.68$ cm. The ratio between the intensities at 90° and 0° of the fibroblast-cell suspension yields 0.555; using the polystyrene-sphere calibration curve (Fig. 8), we find that this corresponds to a particle diameter of 200 nm (±40 nm). The mean diameter of the cells in this particular suspension is 15.2 μm [SD 1.2 μm (7.9%)]. The largest cell observed had a diameter of $d = 22.3$ μm, whereas the smallest cell had a diameter of $d = 8.4$ μm. Therefore it appears that the scattering must be caused by much smaller structures. Fibroblast mitochondria with diameters of[25] 0.05–0.3 μm seem to be the most likely candidates. This would support the findings of a recent study on another mammalian cell by Beauvoit *et al.*[32] Using near-infrared time-resolved spectroscopy to probe rat liver mitochondria and liver-cell suspensions, they conclude that the light scattering from liver cells lies totally in its mitochondria content.

4. Discussion

The experiments on diffuse backreflectance of polarized light reveal distinct differences for three cases: (a) The scattering particle is much smaller, (b) much larger, or (c) similar in size to the wavelength of the probing beam. These differences occur predominately for the case of parallel polarizers [Figs. 5(d)–5(f)], whereas for crossed polarizers, similar azimuthal and radial patterns are observed independently of the ratio of particle size to wavelength [Figs. 5(a)–5(c)]. For crossed polarizers four lobes are always visible, with minima at azimuthal angles of 0° and 90° with respect to the plane of polarization of the incoming beam. In the case of parallel polarizers, a similar pattern is observed for particles much larger than the wavelength; however, the pattern is rotated by 45° [Fig. 5(c)]. If the particles are much smaller than the wavelength, the four-lobe pattern is replaced by a two-lobe pattern, if viewed with a parallel polarizer. Also, small particles have a small g value, and for this case the differences in the size of the pattern are observed depending on whether the polarizers are parallel or crossed. For large g values the diameters of the crossed and the parallel patterns become comparable. The question arises as to why these differences occur.

Differences in the phase functions for different particle sizes account for some of the observed phenomena. Figure 15 displays the three phase functions for the particles in Fig. 5 as calculated by Mie theory.[29] The y axis displays the scattered irradiance per unit of incident irradiance for incident light that is either polarized parallel (p) or orthogonal (s) to the scattering plane. For easier comparison, the scat-

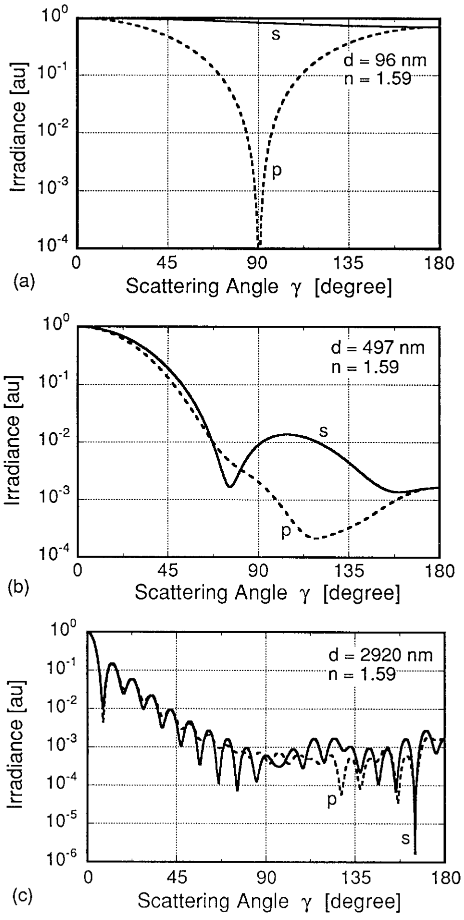

Fig. 15. Mie calculations of the scattering phase function for spherical particles with a refractive index of $n = 1.59$ in H_2O ($n_w = 1.33$) at a wavelength of $\lambda = 632.8$ nm. Diameters d of the particles are (a) 0.096 nm, (b) 497 nm, (c) 2920 nm.

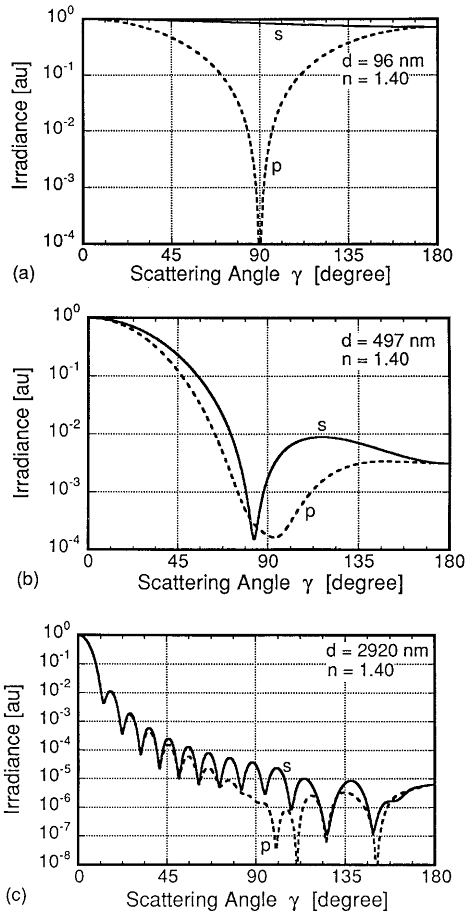

Fig. 16. Same as Fig. 13, except that the spherical particles have a smaller refractive index of $n = 1.4$, which is typical for biological cells and their compartments.

tered irradiance was normalized in all figures to 1 for the scattering angle $\gamma = 0$. The scattering angle γ depicted on the x axis is defined as the angle between the direction of the incident and the scattered wave for a single scattering event. The angle γ is not to be confused with the azimuthal angle α, which was used in the above discussions and figures and, together with r, described a position on the surface of the scattering suspension.

It can be seen that for the small particles with $d =$ 96 nm, a distinct difference for the p and the s components exist. For p scattering there is a sharp minimum at scattering angles close to 90°, which is absent for s scattering. Because the phase functions for the two polarizations are so different, one can expect the diffuse-backscattered signals to be different for crossed and parallel polarizer positions. With increasing particle size this difference becomes less pronounced. For large particles [Fig. 15(c)] there are variations in the high-frequency oscillations of $p(\theta)$, but the overall shapes are similar. Patterns with four lobes are found for both the parallel and the crossed polarizer cases. For a more detailed analysis of the causes for the observed patterns, numerical methods, like Monte Carlo simulations, will be necessary, and we expect to make this the subject of a future paper.

That the pattern for the parallel polarizer case is larger than the pattern with crossed polarizers, if the suspension consists of particles smaller than the wavelength, is in agreement with findings of Yoo and Alfano[13] and MacKintosh *et al.*[33] These groups found that the parallel polarization component for backscattered light is stronger and decays slower than the perpendicular component if suspensions of small spheres are used.

The interpretation of the images from biological-cell suspensions when they are related to findings for polystyrene-sphere suspensions is only approximate. Polystyrene spheres have an index of refraction $n =$ 1.59 at $\lambda = 632.8$ nm. The refractive indices of biological cells and their cell compartments have not yet been studied in detail; however, a couple of studies on various tissues and cell components suggest a range of $n_{\text{cell}} \sim 1.35\text{–}1.51$.[34–38] The differences in the refractive indices between polystyrene spheres and biological cells will result in somewhat different scattering phase functions. To illustrate the effects of a lower index of refraction, Fig. 16 shows the phase functions for the same sphere sizes as in Fig. 15 but with $n = 1.4$. The background medium in both cases is H_2O with $n = 1.33$. When Figs. 15 and 16 are compared, it can be seen that for an increasing particle size the differences in the phase functions increases. However, the general conclusion of the previous paragraph remains. For small particles there is a pronounced difference between the p and the s polarizations, whereas for large particles the p and the s phase functions are similar in shape. Therefore one can expect qualitatively similar results for polystyrene-sphere and biological-cell suspensions.

5. Summary

We have shown that, by probing a turbid medium with a narrow beam of linearly polarized light and viewing the diffuse-backscattered light with crossed and parallel polarizers, we observe azimuthal and radial variations in the intensity around the light input point. Studies with polystyrene-sphere suspensions reveal that, for a given wavelength and refractive index, the structures of these spatially varying intensity patterns depend on particle size, the anisotropy factor g, and the scattering coefficient μ_s. The particle diameter can be deduced from the azimuthal variations of the pattern, and μ_s and g can be determined from the radial extent of the pattern. Experiments with Intralipid, yeast-cell, and fibroblast suspensions demonstrate that these patterns can also be observed in media that contain scattering centers with a range of sizes. The measurements on yeast cells and mammalian fibroblast cells suggest that particles much smaller than the cell volume, possibly mitochondria, cause most of the light scattering. Differences in mitochondria size and concentration are often observed between healthy and diseased cells and tissues.[31] Therefore the method of PDB imaging has the potential of becoming a new diagnostic tool.

The authors thank D. Zerkle for the supply of the CCD camera, J. Hannes for the preparation of the yeast-cell suspensions, and J. P. Freyer for the preparation of the fibroblast suspensions. This work was supported in part by the U.S. Department of Energy.

References

1. W. S. Bickel, J. F. Davidson, D. R. Huffman, and R. Kilkson, "Application of polarization effects in light scattering: a new biophysical tool," Proc. Natl. Acad. Sci. USA **73,** 486–490 (1976).
2. H. C. van de Hulst, *Light Scattering by Small Particles* (Wiley, New York, 1957), 40–59.
3. W. P. van De Merwe, D. R. Huffman, and B. V. Bronk, "Reproducibility and sensitivity of polarized-light scattering for identifying bacterial suspensions," Appl. Opt. **28,** 5052–5057 (1989).
4. B. V. Bronk, W. P. van de Merwe, and M. Stanley, "An *in vivo* measure of average bacterial cell size from polarized light scattering function," Cytometry **13,** 155–162 (1992).
5. B. V. Bronk, S. D. Druger, J. Czege, and W. P. van de Merwe, "Measuring diameters of rod-shaped bacteria *in vivo* with polarized light scattering," Biophys. J. **69,** 1170–1177 (1995).
6. W. S. Bickel and M. E. Stafford, "Polarized light scattering from biological systems: a technique for cell differentiation," J. Biol. Phys. **9,** 53–66 (1981).
7. B. G. deGrooth, L. W. M. M. Terstappen, G. J. Puppels, and J. Greve, "Light-scattering polarization measurements as a new parameter in flow cytometry," Cytometry **8,** 539–544 (1987).
8. G. C. Salzman, S. B. Singham, R. G. Johnston, and C. F. Bohren, "Light scattering and cytometry," in *Flow Cytometry and Sorting*, 2nd ed. (Wiley-Liss, New York, 1990), pp. 81–107.
9. S. Zeitz, A. Belmont, and C. Nicolini, "Differential scattering of circularly polarized light as a unique probe of polynucleosome superstructure," Cell Biophys. **5,** 163–187 (1983).
10. I. J. Tinoco, W. Mickols, M. F. Maestre, and C. Bustamante,

"Absorption, scattering, and imaging of biomolecular structures with polarized light," Ann. Rev. Biophys. Biochem. **16,** 319–349 (1987).

11. M. I. Mishchenko and J. W. Hovenier, "Depolarization of light backscattered by randomly oriented nonspherical particles," Opt. Lett. **20,** 1356–1358 (1995).
12. N. J. McCormick, "Particle-size-distribution retrieval from backscattered polarized radiation measurements: a proposed method," J. Opt. Soc. Am. A **7,** 1811–1816 (1990).
13. K. M. Yoo and R. R. Alfano, "Time resolved depolarization of multiple backscattered light from random media," Phys. Lett. A **142,** 531–536 (1989).
14. R. R. Anderson, "Polarized-light examination and photography of the skin," Arch. Dermatol. **127,** 1000–1005 (1991).
15. L. Wang, D. V. Stephens, S. L. Thomsen, S. L. Jacques, and F. K. Tittel, "Polarized diffuse reflectance of laser light on a turbid medium," presented at the International Conference on Future Directions of Lasers in Surgery and Medicine, Engineering Foundation, Snowbird, Utah, 9–14 July 1995.
16. S. L. Jacques, L. H. Wang, D. V. Stephens, and M. Ostermeyer, "Polarized light transmission through skin using video reflectometry: toward optical tomography of superficial tissue layers," in *Lasers in Surgery: Advanced Characterization, Therapeutics, and Systems VI*, R. R. Anderson, ed., Proc. SPIE **2671,** 199–220 (1996).
17. T. J. Farrell, M. S. Patterson, and B. Wilson, "A diffusion theory model of spatially resolved, steady-state diffuse reflectance for the noninvasive determination of tissue optical properties *in vivo*," Med. Phys. **19,** 879–888 (1992).
18. M. Dogariu and T. Asakura, "Photon pathlength distribution from polarized backscattering in random media," Opt. Eng. **35,** 2234–2239 (1996).
19. W. M. Star, J. P. A. Marijnissen, H. Jansen, M. Keijzer, and M. J. C. van Gemert, "Light dosimetry for photodynamic therapy by whole bladder wall irradiation," Photchem. Photobiol. **46,** 619–624 (1987).
20. C. J. M. Moes, M. J. C. van Gemert, W. M. Star, J. P. A. Marijnissen, and S. A. Prahl, "Measurements and calculations of the energy fluence rate in a scattering and absorbing phantom at 633 nm," Appl. Opt. **28,** 2292–2296 (1989).
21. H. J. van Staveren, C. J. M. Moes, J. van Marle, S. A. Prahl, and M. J. C. van Gemert, "Light scattering in Intralipid-10% in the wavelength range of 400–1100 nm," Appl. Opt. **30,** 4507–4514 (1991).
22. S. T. Flock, S. L. Jacques, B. C. Wilson, W. M. Star, and M. J. C. van Gemert, "Optical properties of Intralipid: a phantom medium for light propagation studies," Lasers Surg. Med. **12,** 510–519 (1992).
23. W. H. Press, B. P. Flannery, S. A. Teukolsky, and W. T. Vetterling, *Numerical Recipes in C* (Cambridge U. Press, New York, 1995), p. 611.
24. B. Beauvoit, H. Liu, K. Kang, P. D. Kaplan, M. Miwa, and B. Chance, "Characterization of absorption and scattering properties for various yeast strains by time-resolved spectroscopy," Cell Biophys. **23,** 91–109 (1994).
25. L. C. Junqueira, J. Carneiro, and R. O. Kelley, *Basic Histology* (Appleton & Lange, Norwalk, Conn., 1992), pp. 108–110.
26. J. P. Freyer, "Rates of oxygen consumption for proliferating and quiescent cells isolated from multicellular tumor spheroids," Adv. Exp. Med. Biol. **345,** 335–342 (1994).
27. W. K. Pratt, *Digital Image Processing* (Wiley, New York, 1991), pp. 285–302.
28. A. K. Jain, Fundamentals of Digital Image Processing (Prentice-Hall, Englewood Cliffs, N.J., 1989), pp. 241–242.
29. C. F. Bohren and D. R. Huffman, *Absorption and Scattering of Light by Small Particles* (Wiley, New York, 1983), pp. 82–129.
30. A. H. Cook, *The Chemistry and Biology of Yeast* (Academic, New York, 1958), p. 235.
31. E. A. Munn, *The Structure of Mitochondria* (Academic, New York, 1974).
32. B. Beauvoit, T. Kitai, and B. Chance, "Contribution of the mitochondrial compartment to the optical properties of the rat liver: a theoretical and practical approach," Biophys. J. **67,** 2501–2510 (1994).
33. F. C. MacKintosh, J. X. Zhu, D. J. Pine, and D. A. Weitz, "Polarization memory of multiply scattered light," Phys. Rev. B **40,** 9342–9345 (1989).
34. A. Brunsting and P. F. Mullaney, "Differential light scattering from spherical mammalian cells," Biophys. J. **14,** 439–453 (1974).
35. S. Fujime, M. Takasaki-Oshito, and S. Miyamoto, "Dynamic light scattering from polydisperse suspensions of large spheres," Biophys. J. **54,** 1179–1184 (1988).
36. R. C. Weast, ed., *CRC Handbook of Chemistry and Physics* (CRC Press, Boca Raton, Fla., 1989).
37. F. A. Duck, *Physical Properties of Tissue* (Academic, London, 1990), p. 63.
38. H. Li and S. Xie, "Measurement method of the refractive index of biotissue by total internal reflection," Appl. Opt. **35,** 1793–1795 (1996).